Available online at www.sciencedirect.com
ScienceDirect
Journal of Molecular Catalysis A: Chemical 258 (2006) 124–132
JOURNAL OF MOLECULAR CATALYSIS A: CHEMICAL
www.elsevier.com/locate/molcata

Nano-Ag particles doped TiO_2 for efficient photodegradation of Direct azo dyes

N. Sobana, M. Muruganadham [1], M. Swaminathan *

Department of Chemistry, Annamalai University, Annamalai Nagar 608002, India

Received 22 September 2005; received in revised form 29 April 2006; accepted 4 May 2006
Available online 23 June 2006

Abstract

Silver nanoparticles doped TiO_2 has been prepared and characterised by surface analytical methods such as BET surface area, scanning electron micrographs (SEM), X-ray diffraction (XRD), energy dispersive X-ray micro analysis (EDX), electron spin resonance (ESR) and diffuse reflectance spectroscopy (DRS). We have investigated the photocatalytic degradation of two Direct diazo dyes, Direct red 23 (DR 23) and Direct blue 53 (DB 53) in the aqueous suspensions of TiO_2 and Ag deposited TiO_2 nanoparticles under UV-A light irradiation in order to evaluate the various effects of silver deposition on the photocatalytic activity of TiO_2. The presence of silver in TiO_2 was found to enhance the photodegradation of DR 23 and DB 53. The higher activity of silver doped TiO_2 is due to the enhancement of electron–hole separation by the electron trapping of silver particles.

Keywords: Silver nanoparticle doping; TiO_2; Direct blue 53; Direct red 23; UV-A light; Photocatalysis

1. Introduction

Heterogeneous photocatalysis is an alternative economical and harmless technology of advanced oxidation processes (AOP) for removal of organic impurities. During the process, illuminated semiconductor absorbs light and generates active species which leads to complete oxidation of organic components in waste water. A distinct advantage of the photocatalysis lies in its ability to utilise solar energy in the production of active species $OH^{\bullet}$. Photocatalysis on semiconductors has been studied in many fields. For example: (i) fuel production: hydrogen from water photolysis [1–3], (ii) removal/recovery of heavy metal ions [4,5], (iii) water detoxification: removal of toxic, harmful or hazardous pollutants [6–11].

A great many photocatalysts have been examined for the degradation of organic pollutants in waste water. Among various semiconductor metal oxides, TiO_2 has been the focus of photocatalysts under UV irradiation because of its physical and chemical stability, low cost, ease of availability, non-toxicity and electronic and optical properties. Despite the positive attributes of TiO_2, there are a few drawbacks associated with its use; it has a high bandgap ($E_g > 3.2$ eV) and it is excited only by UV light ($\lambda < 388$ nm) to inject electrons into the conduction band and to leave holes into the valence band [12]. Thus, this practically limits the use of sunlight or visible light as an irradiation source in photocatalytic reactions on TiO_2 [13]. In addition, the high rate of electron–hole recombination on TiO_2 particles results in a low efficiency of photocatalysis [14]. For the purpose of overcoming these limitations of TiO_2 as a photocatalyst, numerous studies have been recently performed to enhance electron–hole separation and to extend the absorption range of TiO_2 into the visible range. These studies include doping metal ions into the TiO_2 lattice [15,16], dye photosensitisation on the TiO_2 surface [17–21], addition of inert support [22] and deposition of noble metals [23–34].

In particular, noble metal-modified semiconductor nanoparticles become of current importance for maximising the efficiency of photocatalytic reactions. The noble metals such as Pt [23,24] and Au [25,26] deposited or doped on TiO_2 have the high Schottky barriers among the metals and thus act as electron traps, facilitating electron–hole separation and promotes the interfacial electron transfer process [5,35–37]. Most studies of noble metal-modified TiO_2 photocatalysts have focused

* Corresponding author. Tel.: +91 4144 220572; fax: +91 4144 238080.
E-mail address: chemsam@yahoo.com (M. Swaminathan).
[1] Present address: Department of Environmental Engineering and Science, Feng chia University, Taichung, Taivan.

1381-1169/$ – see front matter © 2006 Elsevier B.V. All rights reserved.
doi:10.1016/j.molcata.2006.05.013

on the details of the photoinduced electron transfer from the conduction band of UV-irradiated TiO_2 to noble metals for improving the photocatalytic activity of TiO_2 under UV irradiation.

Noble metals doped or deposited on TiO_2 are expected to show various effects on the photocatalytic activity of TiO_2 by different mechanisms. These noble metals act separately or simultaneously depending on the photoreaction conditions. They may (i) enhance the electron–hole separation by acting as electron traps, (ii) extend the light absorption into the visible range and enhance surface electron excitation by plasmon resonances excited by visible light and (iii) modify the surface properties of photocatalysts.

In the recent years, silver ions have attracted the interests of several researchers [38–40], because of both their novel effects on the improvement of photoactivity of semiconductor photocatalysis nanocrystallites [39,40] and their effects on antibacterial activity [38]. These properties can be applied to a tremendous range of applications, for instance, environment, textiles, engineering materials and so on. However, the studies on silver doped photocatalyst nanocrystallites are still limited in the literature [41–49].

The aim of the present work is to prepare Ag doped TiO_2 (anatase) by a photodeposition method and to compare the activity of the photocatalyst before and after surface modification with metallic silver for the degradation of two azo dyes DB 53 and DR 23.

2. Experimental

2.1. Materials

Titanium dioxide (anatase) with a BET surface area of 21.53 m^2/g and perchloric acid were supplied by Qualigen. Direct red 23 (DR 23), C.I. 29160 from S.D. fine and Direct blue 53 (DB 53) C.I. 23860 from CDH were used as such. The structure of these dyes are shown in Fig. 1. Silver nitrate (99.5 wt.%) analytical grade from Merck was used as a silver source for the preparation of Ag doped TiO_2 photocatalysts. Double distilled water was used for all the experiments.

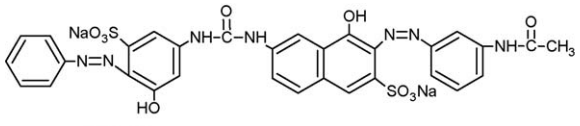

Structure of DR 23

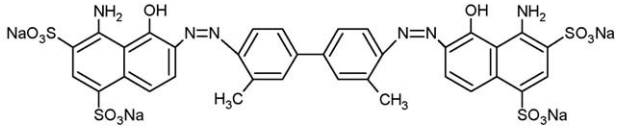

Structure of DB53

Fig. 1. Structures of DR23 and DB53.

2.2. Preparation of Ag doped TiO_2 photocatalysts

The Ag doped TiO_2 catalysts were prepared by photoreducing Ag^+ ions to Ag metal on the TiO_2 surface as per the procedure given below [41].

First pH of the TiO_2 suspension was adjusted to 3 prior to reaction using perchloric acid. Aliquots of various amounts of Ag^+ ions, prepared by dissolving silver nitrate salt in deionised water, were added into the suspension of TiO_2 such that the Ag^+ concentration was 0.5, 1.0, 1.5 and 2.0 at.% in relation to TiO_2. The mixtures were then irradiated with UV light by eight mercury lamps (8 W) for 3 h with continuous air supply. The suspensions were then filtered, washed and dried to give Ag deposited TiO_2 catalysts.

2.3. Analytical methods

A Varian Cary 5E UV–VIS-NIR spectrophotometer equipped with an integrated sphere was used to record the diffuse reflectance spectra (DRS) and to measure the absorbance data of the solution samples. The baseline correction was performed using a calibrated reference sample of barium sulfate. The reflectance spectra of the silver doped TiO_2 catalysts were analysed under ambient conditions in the wavelength range of 200–800 nm.

Powder X-ray diffraction patterns of TiO_2 and Ag doped TiO_2 catalysts were obtained using a Philips PANanalytical X′ pert PRO diffractometer equipped with a Cu tube for generating a Cu Kα radiation (wavelength 1.5406 Å) at 40 kV, 25 mA. The particles were spread on a glass slide specimen holder and the scattered intensity was measured between 20° and 85° at a scanning rate of $2\theta = 1.2^\circ\ min^{-1}$. Peak positions were compared with the standard files to identify the crystalline phases.

The electron paramagnetic resonance (EPR) spectra of the silver doped TiO_2 catalysts were recorded by using a JEOL-JE 100 ESR spectrometer at room temperature. The TiO_2 powder was placed in a thin-walled quartz EPR tube to produce cylindrical samples with identical dimensions. The EPR spectrometer settings were microwave power of 1.00 mW, microwave frequency of 9.39 GHz. Center field of 335 ± 100 mT, modulation amplitude of 0.2 mT and scan time of 0.03 s.

Scanning electron microscopic (SEM) analysis was performed on platinum coated samples using a JEOL apparatus model JSM-5610 LV, equipped with an INCA EDX probe for the energy dispersive X-ray micro analysis (EDX).

The specific surface areas of the samples were determined through nitrogen adsorption at 77 K on the basis of BET equation using a Sorptomatic 1990 instrument.

2.4. Photocatalytic studies

The photocatalytic experiments were carried out in a Heber multilamp photoreactor model HML-MP 88 (Fig. 2) which consists of eight medium pressure mercury vapour lamps (8 W) set in parallel and emitting 365 nm wavelength. It has a reaction chamber with specially designed reflectors made of highly polished aluminium and built in cooling fan at the bottom.

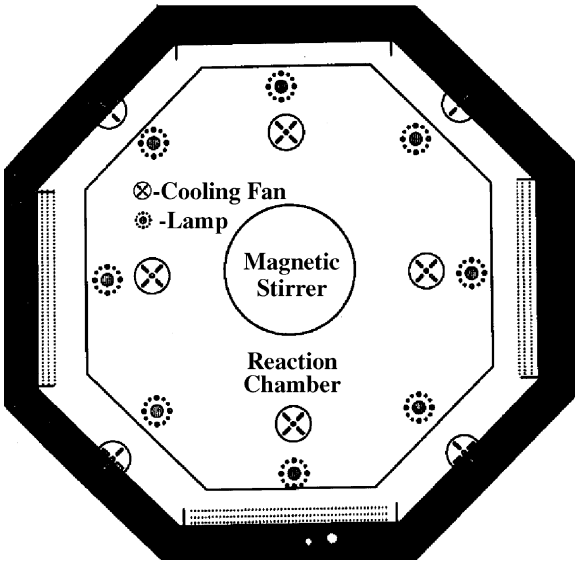

Fig. 2. Scheme of the photoreactor used for the photocatalytic experiments.

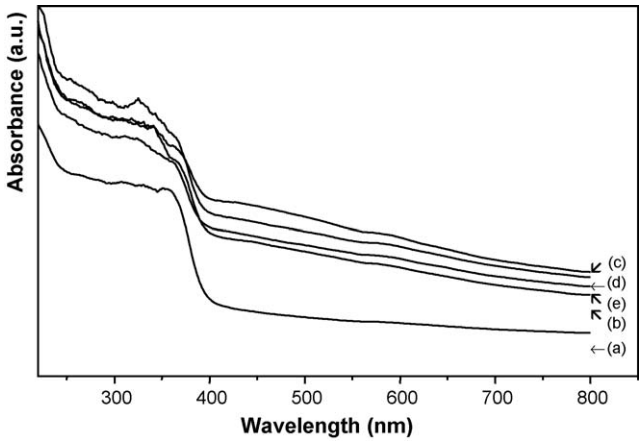

Fig. 3. Diffuse reflectance spectra of the catalysts. (a) Pure TiO_2; (b) 0.5% Ag-TiO_2; (c) 1% Ag-TiO_2; (d) 1.5% Ag-TiO_2; (e) 2% Ag-TiO_2.

Open borosilicate glass tube of 50 ml capacity, 40 cm height and 20 mm diameter with the total light exposure length of 330 nm was used as a reaction vessel. The solution with a photocatalyst and dye was continuously aerated by a pump to provide oxygen and for complete mixing of reaction mixture.

For photocatalysis, 50 ml of dye solution containing appropriate quantity of the catalyst suspensions was used. The suspension was stirred for 30 min in dark for the attainment of adsorption equilibrium and then irradiated. At specific time intervals 2 ml of the sample was withdrawn and centrifuged to separate the catalyst. 1 ml of the centrifugate was diluted to 10 ml and its absorbances at 501 and 242 nm for DR 23, 603 and 315 nm for DB 53 were measured using a Hitachi U-2001 spectrophotometer. The absorbances at 501 and 603 nm were used to monitor the decolourisation of the dyes and the absorbances at 242 and 315 nm indicate the degradation of aromatic part of dyes.

The initial pH of the working samples were adjusted to 5 by the addition of H_2SO_4 or NaOH solution using a Hanna Phep (Model H 198107) digital pH meter.

3. Results and discussion

3.1. Characterisation of TiO_2 and Ag-TiO_2 catalysts

3.1.1. UV–visible diffuse reflectance spectra

The reflectance spectra of TiO_2 and 0.5, 1, 1.5 and 2 at.% of Ag doped TiO_2 catalysts are illustrated in Fig. 3. The spectrum of TiO_2 consists of a single absorption below ca. 370 nm usually ascribed to charge-transfer from the valence band (mainly formed by 2p orbitals of the oxide anions) to the conduction band (mainly formed by $3d_{t2g}$ orbitals of the Ti^{4+} cations) [50]. The addition of silver ions and subsequent UV irradiation causes significant changes to the absorption spectrum of TiO_2 resulting in high absorbance from 400 nm to entire visible region which is characteristic of surface plasmon absorption. A band at 440 nm is characteristic of surface plasmon absorption. Since this band does not appear as a strong band as reported in literature [47,51], the red shift may not be due to surface plasmon absorption. Hence the extended absorption must be from bandgap absorption. This bandgap absorption of all silver doped TiO_2 catalysts slightly shifts to higher wavelength. The absorbance in the visible region for the metallised system shows that lower energy transitions are possible. This is because the metal clusters give rise to localised energy levels in the bandgap of TiO_2 into which valence band electrons of TiO_2 are excited at wavelength longer than 370 nm. If equal sized metal clusters are formed, it will lead to constant absorption in the visible region corresponding to the excitation from the valence band of TiO_2 to the unoccupied level of metal cluster. Since there is a small gradual decrease in absorption from 420 to 800 nm in the diffuse reflectance spectrum of Ag-TiO_2 catalyst, the metal clusters in the catalyst are not be of equal size.

The spectra reveals that Ag doping has a marked effect on the absorption properties of TiO_2 and that the absorption of light in the visible region by TiO_2 increases with an increase in the silver content.

3.1.2. XRD analysis

XRD patterns of TiO_2 and Ag-TiO_2 nanocrystallites with different contents of silver ions are shown in Fig. 4. The X-ray diffraction patterns of silver doped TiO_2 samples almost coincide with that of pure TiO_2 and show no diffraction peaks due to silver species, thus suggesting that the metal particles are well dispersed on the TiO_2 surface. Anatase type structure is kept in all Ag doped TiO_2 catalysts, indicating that the metal dopants are merely placed on the surface of the crystals without being covalently anchored into the crystal lattice. There are no diffraction patterns characteristic of the doped metals in the XRD patterns. Hence these metal sites are expected to be below the visibility limit of X-ray analysis [52].

The crystallite size was determined from the diffraction peak broadening employing the following equation:

$$D = \frac{K\lambda}{(\beta_c - \beta_s)\cos\theta}$$

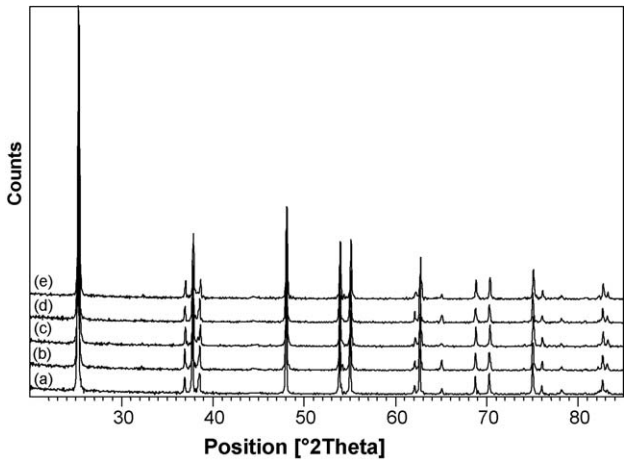

Fig. 4. XRD patterns of the catalysts. (a) Pure TiO_2; (b) 0.5% Ag-TiO_2; (c) 1% Ag-TiO_2; (d) 1.5% Ag-TiO_2; (e) 2% Ag-TiO_2 catalysts.

where D is the crystallite size of the catalyst, λ the X-ray wavelength, and β_c and β_s are the FWHM of the catalyst and the standard, respectively. $K = 0.89$ is a coefficient and θ is the diffraction angle.

The crystallite sizes determined from the XRD pattern of the prepared catalysts are given in Table 1. It is noted that all the catalysts are in the form of nanoparticulates with sizes ranging from 21 to 40 nm. The crystallite size of Ag-TiO_2 samples are larger than pure TiO_2. The decrease in crystallite size is inversely proportional to the surface of the catalysts.

3.1.3. ESR analysis

The formation of active species on metal deposited TiO_2 and pure TiO_2 can be found by ESR spectra. ESR spectra of these photocatalysts were recorded at room temperature. In the ESR spectrum for the pure TiO_2 (Fig. 5), simple signals at $g = 1.96$, 1.97, 1.99 and 2.04 were observed. The signals were not ascribed completely; however they seem to be a combination of signals for Ti^{3+} ($g = 1.96$, 1.97, 1.99) and $O_2^{\bullet -}$ ($g = 2.04$) [53–55]. Obvious differences were not observed in the ESR spectra of Ag-TiO_2 nanocrystallites with different contents of silver and TiO_2 recorded at room temperature [56]. This indicates the active species present in TiO_2 and Ag doped TiO_2 are the same.

3.1.3.1. SEM analysis. We observed maximum efficiency for 1.5 and 2 at.% of Ag doped TiO_2 in the photocatalytic degradation of DR 23 and DB 53, respectively. Hence SEM analysis has been carried out for these two catalysts. The SEM pictures of pure TiO_2, 1.5 at.% Ag-TiO_2 and 2 at.% Ag-TiO_2 are shown in Fig. 6. The SEM picture of pure TiO_2 (Fig. 6a) shows that the size of titanium dioxide particle is uniform. But the distribution of silver on the surface of TiO_2 is not uniform and the SEM pictures (Fig. 6b and c) show that Ag doped TiO_2 catalyst contains irregular shaped particles which are the aggregation of tiny crystals. However, it cannot be ruled out that some Ag particles are too small to be observed at the resolution of the used microscope [45,46,52]. The above figures also reveal that the doping of silver metal does not leave any change in the topology of the catalyst surface.

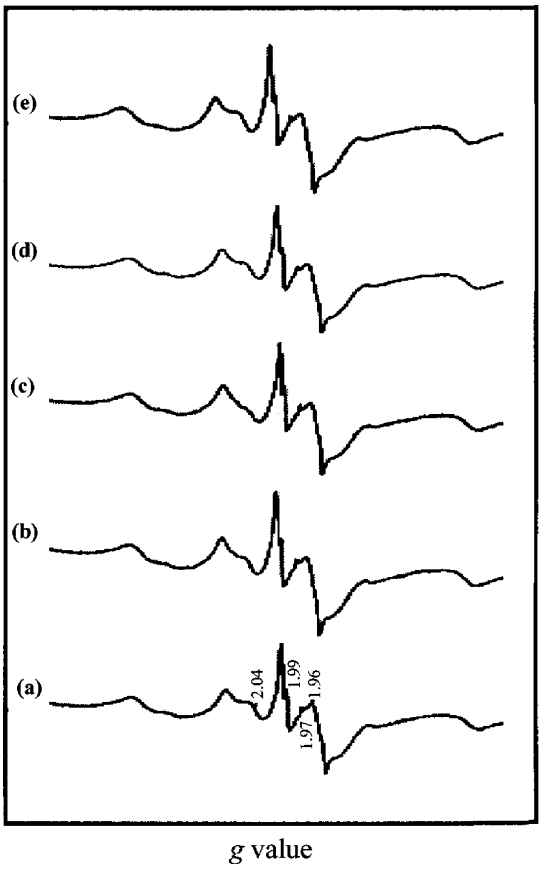

Fig. 5. ESR spectra of the catalysts. (a) Pure TiO_2; (b) 0.5% Ag-TiO_2; (c) 1% Ag-TiO_2; (d) 1.5% Ag-TiO_2; (e) 2% Ag-TiO_2 catalysts recorded at room temperature.

Table 1
Crystallite size and photocatalytic activity results of TiO_2 and Ag doped TiO_2 on DR 23

Catalyst amount (2 g l^{-1})	Ag weight (%)	Crystallite size (nm)	Degradation		Decolourisation	
			$k \times 10^1$ (min^{-1})	$R \times 10^5$ (mol l^{-1} min^{-1})	$k \times 10^1$ (min^{-1})	$R \times 10^5$ (mol l^{-1} min^{-1})
TiO_2	0.0	20.85	2.10	4.2	12.62	25.2
Ag-TiO_2	0.5	31.28	2.35	4.7	12.88	25.8
Ag-TiO_2	1.0	34.57	3.98	7.96	13.24	26.5
Ag-TiO_2	1.5	39.28	6.10	12.2	13.46	26.9
Ag-TiO_2	2.0	32.29	4.82	9.64	13.28	26.7

k = *Pseudo*-first order rate constant; R = initial rate.

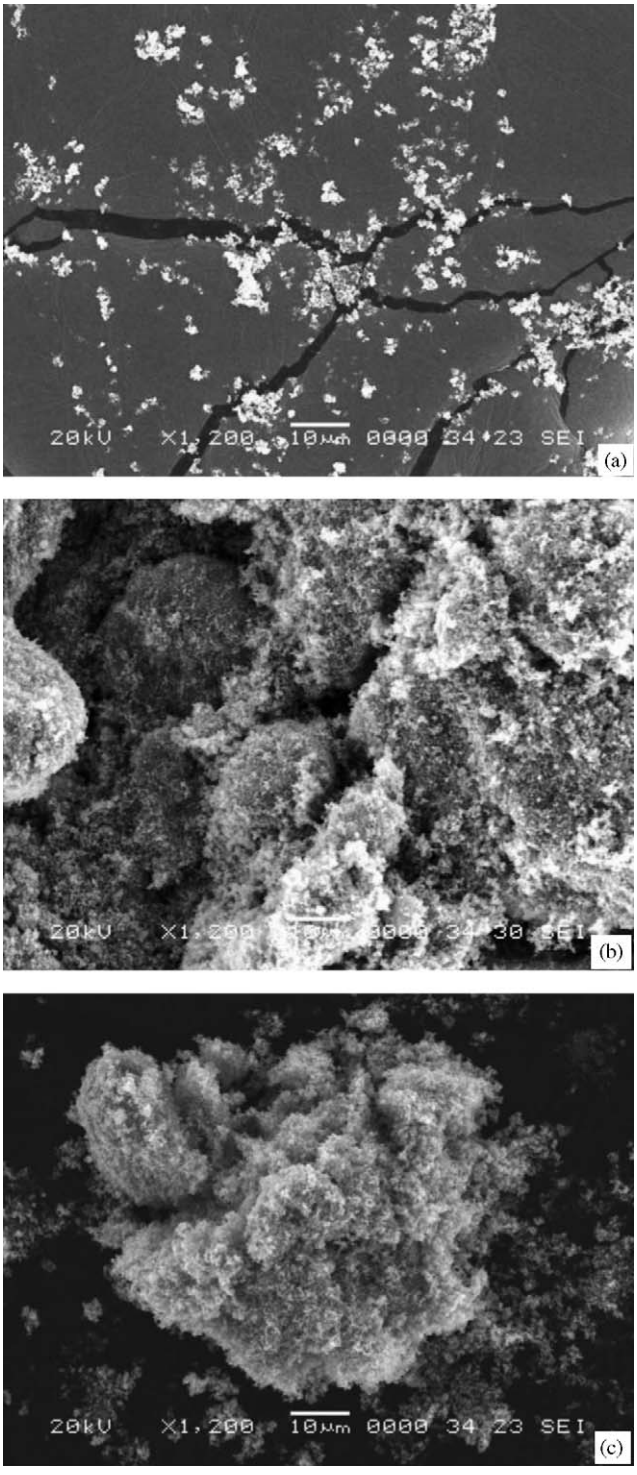

Fig. 6. Scanning electron micrograph image of the catalysts. (a) Pure TiO_2; (b) 1.5% Ag-TiO_2; (c) 2% Ag-TiO_2 catalysts.

3.1.3.2. EDX analysis. We have also performed EDX analysis on the Ag doped TiO_2 catalyst in two different regions I and II. They are presented in Figs. 7 and 8. From Fig. 7a and b we notice that, in 1.5 at.% Ag-TiO_2 the Ag content of 7.49 wt.% (region I) falls to 0.94 wt.% in the region II. In the case of 2 at.% Ag-TiO_2 catalyst (Fig. 8a and b) Ag is 2.09 wt.% in region I and it is raised to 6.88 wt.% in the region II. This

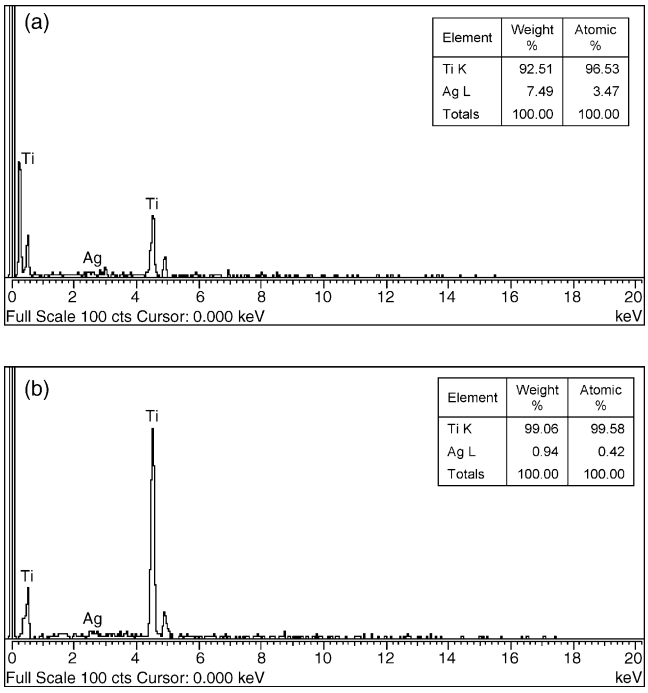

Fig. 7. EDX diagrams of 1.5% Ag-TiO_2 catalyst obtained from two different regions. (a) Region I; (b) region II.

confirms that the size and deposition of silver on TiO_2 is non-uniform.

3.1.4. BET surface area analysis

In general, the surface area of the catalyst is the most important factor influencing the catalytic activity. The surface area of TiO_2 particles before and after surface modification was deter-

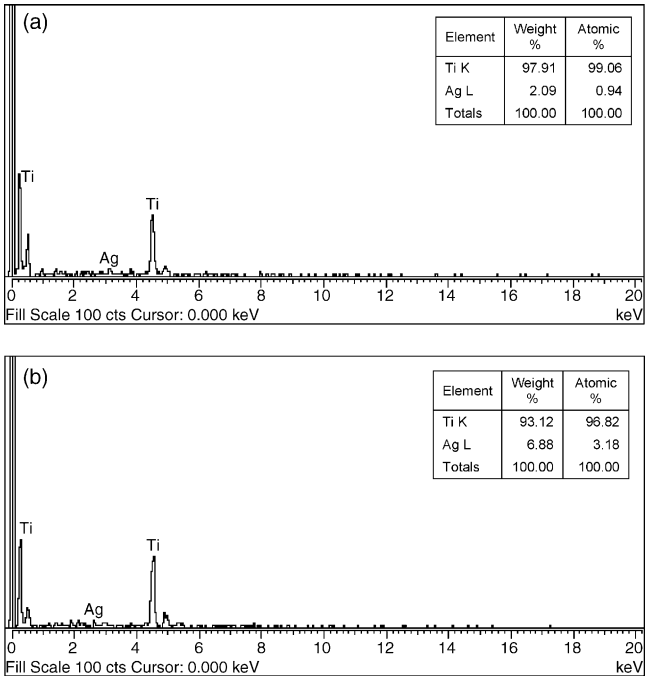

Fig. 8. EDX diagrams of 2% Ag-TiO_2 catalyst obtained from two different regions. (a) Region I; (b) region II.

Table 2
BET surface area of pure and silver doped TiO_2 catalysts

Catalyst	Ag weight (%)	BET surface area (m^2/g)
TiO_2	0.0	21.53
Ag-TiO_2	1.5	17.78
Ag-TiO_2	2.0	12.39

mined using the nitrogen gas adsorption method. The surface areas obtained are shown in Table 2.

It is observed that the surface area decreases with an increase in the silver content in the Ag-TiO_2 catalyst. The decrease in the surface area of silver doped TiO_2 may be due to blocking of fine capillaries of parent TiO_2 surface by metal film islands [52].

3.2. Comparison of photocatalytic activities of TiO_2 and Ag doped TiO_2 catalysts

3.2.1. DR 23 photodegradation

Fig. 9 shows the spectral changes of DR 23 in TiO_2 photocatalyst under UV irradiation. Compared to pure TiO_2, the Ag-TiO_2 catalysts exhibited a significant increase in the DR 23 photodegradation and decolourisation rate as shown in Fig. 10a and b. In Table 1 crystallite size and photocatalytic activity of TiO_2 and Ag doped TiO_2 on DR 23 are given. It was found that the 1.5 at.% Ag content was optimum to achieve the highest efficiency of the DR 23 photodegradation and decolourisation. It is also observed that the photonic efficiency increases with an increase in the silver loading up to 1.5 at.% (optimum metal loading) and then decreases. More Ag contents could be detrimental to the photonic efficiency. It may be explained that up to optimum metal loading, the Ag particles deposited on the TiO_2 surface can act as electron–hole separation centers [5,35,36]. The electron transfer from the TiO_2 conduction band to metallic silver particles at the interface is thermodynamically possible because the Fermi level of TiO_2 is higher than that of silver metals [23]. This results in the formation of Schottky barrier at the metal–semiconductor contact region, which improves the charge separation and thus enhances the photocatalytic activity

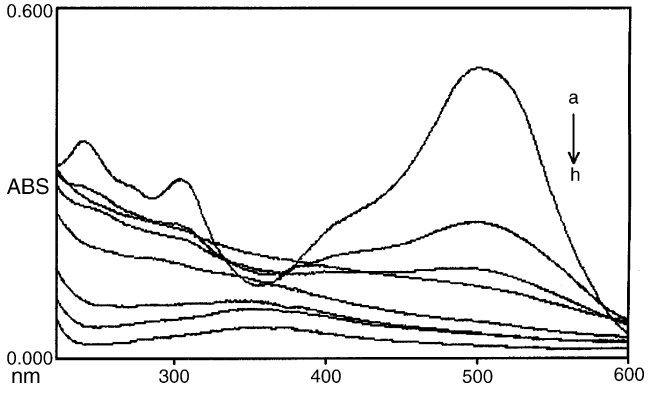

Fig. 9. Absorption spectral changes of DR 23 on pure TiO_2 as a function of irradiation time. The initial concentration (C_0) of DR 23 was 2×10^{-4} mol l^{-1}: (a) 0 min; (b) 60 min; (c) 90 min; (d) 120 min; (e) 180 min; (f) 210 min; (g) 330 min; (h) 480 min.

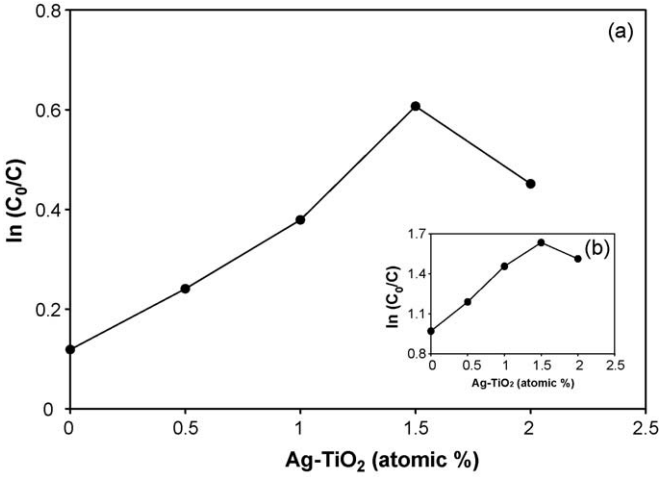

Fig. 10. Photocatalytic (a) degradation; (b) decolourisation of DR 23 in Ag-TiO_2 catalysts as a function of the Ag content (2 h irradiation).

of TiO_2. In contrast, at the Ag content above its optimum, the Ag particles can also act as recombination centers, thereby decreasing the photocatalytic activity of TiO_2. It has been reported that the probability for the hole capture is increased by the large number of negatively charged silver particles on TiO_2 at high silver content, which reduces the efficiency of charge separation [23,42,57–59]. The photodecolourisation and degradation of DR 23 against the irradiation time are shown in Fig. 11a and b. An optimum loading of 1.5 at.% Ag showed 34.3% increase in the DR 23 degradation and 20.3% increase in the decolourisation.

3.2.2. DB 53 degradation

Absorption spectral changes of DB 53 on the TiO_2 catalyst as a function of the irradiation time is shown in Fig. 12. The results of photodegradation and decolourisation of DB 53 using pure TiO_2 and silver doped TiO_2 are shown in Fig. 13a and b. The rate constants and the initial rates of degradation and decolourisation by TiO_2 and doped catalysts are given in Table 3. The photodegradation efficiency increases with an increase in the

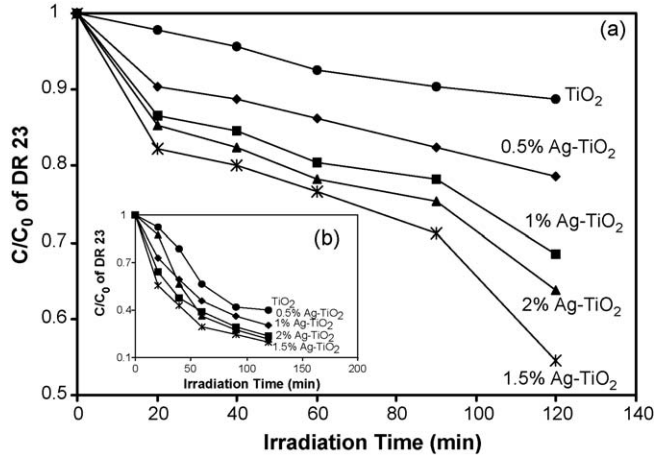

Fig. 11. Comparison of DR 23 photocatalytic: (a) degradation; (b) decolourisation on pure TiO_2 and Ag-TiO_2 catalysts under UV irradiation.

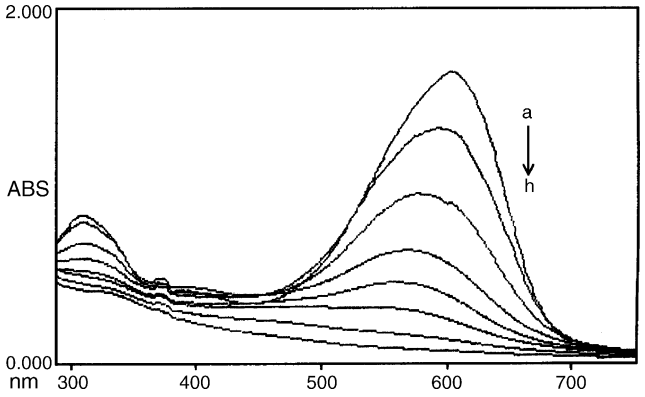

Fig. 12. Absorption spectral changes of DB 53 on pure TiO_2 as a function of irradiation time. The initial concentration (C_0) of DB 53 was 3×10^{-4} mol l^{-1}: (a) 0 min; (b) 60 min; (c) 90 min; (d) 120 min; (e) 180 min; (f) 210 min; (g) 330 min; (h) 480 min.

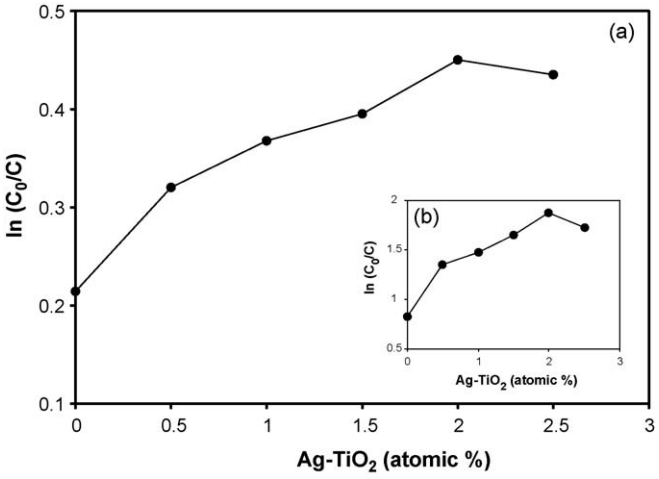

Fig. 13. Photocatalytic (a) degradation; (b) decolourisation of DB 53 on Ag-TiO_2 catalysts as a function of the Ag content (2 h irradiation).

silver loading up to 2% and then decreases. The reason for this enhancement is the same as discussed earlier in the photodegradation of DR 23. The photodecolourisation and degradation of DB 53 against the irradiation time are shown in Fig. 14a and b. An optimum loading of 2.0 at.% Ag showed 17.0% increase in the DB 53 degradation and 28.1% increase in the decolourisation.

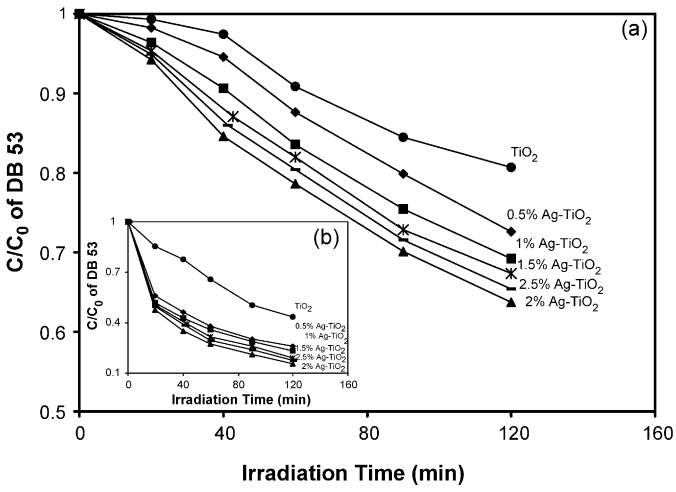

Fig. 14. Comparison of DB 53 photocatalytic (a) degradation; (b) decolourisation on pure TiO_2 and Ag-TiO_2 catalysts under UV irradiation.

3.3. Roles of Ag nanoparticles deposited on TiO_2

The enhancement of photocatalytic activity of TiO_2 in the oxidative degradation of DR 23 and DB 53 by the Ag deposition may be through the following mechanisms.

(i) Ag nanoparticles deposited on TiO_2 act as electron traps, enhancing the electron–hole separation and the subsequent transfer of the trapped electron to the adsorbed O_2 acting as an electron acceptor [5,35–37].
(ii) More dye molecules are adsorbed on the surface of Ag-TiO_2 than on the TiO_2 surface, enhancing the photoexcited electron transfer from the visible light sensitised dye molecule to the conduction band of TiO_2 and subsequently increasing the electron transfer to the adsorbed O_2.

TiO_2-sensitisation pathways for the photodegradation under UV irradiation is shown in Fig. 15. The valence electrons of TiO_2 catalyst are excited to the conduction band by UV light and after various other events, electrons on the TiO_2 particle surface are scavenged by the molecular oxygen to produce reactive oxygen radicals, whereas the valence hole become trapped as the surface-bound $OH^{\bullet}$ radicals on oxidation of either the surface OH group and/or the surface H_2O molecules. Therefore, the charge separation on TiO_2 is a crucial factor in affecting the efficiency of the photodegradation under UV irradiation.

Table 3
Photocatalytic activity of TiO_2 and Ag doped TiO_2 on DB 53

Catalyst amount (2 g l^{-1})	Ag weight (%)	Degradation		Decolourisation	
		$k \times 10^1$ (min^{-1})	$R \times 10^5$ (mol l^{-1} min^{-1})	$k \times 10^1$ (min^{-1})	$R \times 10^5$ (mol l^{-1} min^{-1})
TiO_2	0.0	4.60	13.79	10.60	31.79
Ag-TiO_2	0.5	6.08	18.23	11.60	34.81
Ag-TiO_2	1.0	6.36	19.08	11.70	35.11
Ag-TiO_2	1.5	6.41	19.22	12.29	36.86
Ag-TiO_2	2.0	6.85	20.55	12.63	37.88
Ag-TiO_2	2.5	6.72	20.02	12.34	37.02

k = *Pseudo*-first order rate constant; R = initial rate.

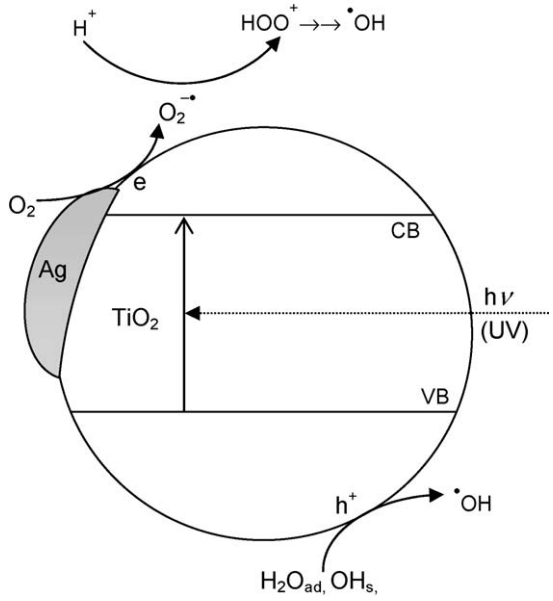

Fig. 15. TiO_2-photosensitisation pathway under UV irradiation.

For the photodegradation of these two Direct dyes on Ag-TiO_2 under UV irradiation, Ag metals act as electron traps thereby enhancing the charge separation. To find out the mechanism, we have also carried out the adsorption experiments. It is found that there is no significant difference in the adsorption of dyes between TiO_2 and Ag-TiO_2 catalysts. So the mechanism (2) is ruled out. Hence the increase in efficiency by Ag deposition is due to the mechanism (1) and it is applicable to the effect of Ag deposits thus leading to the increase in the Ag-TiO_2 photocatalytic activity under UV irradiation.

4. Conclusion

The characterisation of silver doped TiO_2 and TiO_2 using diffuse reflectance spectroscopy, XRD, SEM, EDX and BET surface area techniques revealed the dispersion of silver metal on the surface of TiO_2. The silver doped TiO_2 catalysts shows an absorption threshold extended into the visible region. It is obvious that the Ag clusters give rise to localised energy levels in the bandgap of TiO_2 into which the valence band electrons of TiO_2 are excited at wavelength longer than 370 nm. The photonic efficiency increases with an increase in the metal loading up to an optimum level due to the effect of decreasing recombination of electron and hole. Above the optimum metal loading, the dopants behave as electron/hole recombination centers. Under UV irradiation, Ag deposits exhibit the effect only as electron traps, thus leading to the enhancement in the Ag-TiO_2 photocatalytic activity.

References

[1] A. Fujishima, K. Honda, Bull. Chem. Soc. Jpn. 44 (1971) 1148.
[2] A. Fujishima, K. Honda, Nature (London) 238 (1972) 37.
[3] A.J. Bard, Ber. Bunsenges Phys. Chem. 92 (1988) 1187.
[4] N. Serpone, E. Borgarello, M. Barbeni, E. Pelizzetti, P. Pichat, J.M. Herrmann, M.A. Fox, J. Photochem. Photobiol. A Chem. 36 (1987) 373.
[5] J. Herrmann, J. Disdier, P. Pichat, J. Phys. Chem. 90 (1986) 6028.
[6] R.W. Matthews, S.R. McEvoy, J. Photochem. Photobiol. A Chem. 64 (1992) 231.
[7] H. Gerisher, Electrochim. Acta 38 (1993) 3.
[8] A. Sobczynski, A. Dobosz, Pol. J. Environ. Stud. 10 (2001) 195.
[9] O. Legrini, E. Oliveros, A.M. Braun, Chem. Rev. 93 (1993) 671.
[10] M. Muruganandham, M. Swaminathan, Solar Energy Mater. Solar Cells 81 (2004) 439.
[11] M. Muruganandham, M. Swaminathan, Dyes Pigments 68 (2006) 133.
[12] C. Kormann, D.W. Bahnemann, M.R. Hoffmann, J. Phys. Chem. 92 (1988) 5196.
[13] D.Y. Goswami, J. Sol. Energy 119 (1997) 101.
[14] A. Linsebigler, G. Lu, J.T. Yates, Chem. Rev. 95 (1995) 735.
[15] S.D. Mo, L.B. Lin, J. Phys. Chem. Solids 55 (1994) 1309.
[16] W. Choi, A. Termin, M.R. Hoffmann, J. Phys. Chem. 98 (1994) 13669.
[17] K. Vinodgopal, D.E. Wynkoop, P.V. Kamat, Environ. Sci. Technol. 30 (1996) 1660.
[18] J. Zhao, T. Wu, K. Wu, K. Oikawa, H. Hidaka, N. Serpone, Environ. Sci. Technol. 32 (1998) 2394.
[19] A. Fujishima, T.N. Rao, D.A. Tryk, J. Photochem. Photobiol. C Photochem. Rev. 1 (2000) 1.
[20] T. Wu, G. Liu, J. Zhao, H. Hidaka, N. Serpone, J. Phys. Chem. B 102 (1998) 5845.
[21] G. Liu, T. Wu, T. Lin, J. Zhao, Environ. Sci. Technol. 33 (1999) 1379.
[22] J. Matos, J. Laine, J.M. Herrmann, Carbon 37 (1999) 1870.
[23] A. Sclafani, J.M. Herrmann, J. Photochem. Photobiol. A Chem. 113 (1998) 181.
[24] A. Wold, Chem. Mater. 5 (1993) 280.
[25] V. Subramanian, E. Wolf, P. Kamat, J. Phys. Chem. B 105 (2001) 11439.
[26] C.Y. Wang, C.Y. Liu, X. Zheng, J. Chen, T. Shen, Colloid Surf. A 131 (1998) 271.
[27] W. Mu, J.M. Herrmann, P. Pichat, Catal. Lett. 3 (1989) 73.
[28] K. Chiang, R. Amal, T. Tran, Adv. Environ. Res. 6 (2002) 471.
[29] S. Sakthivel, S.U. Geissen, D.W. Bahnemann, V. Murugesan, A. Vogelpohl, J. Photochem. Photobiol. A Chem. 148 (2002) 283.
[30] A. Dipaola, E. Garicia-Lopez, S. Ikeda, G. Marci, B. Ohtani, L. Palmisano, Catal. Today 75 (2002) 87.
[31] A. Dobosz, A. Sobczynski, Water Res. 37 (2003) 1489.
[32] D. Hufschmidt, D. Bahnemann, J.J. Testa, C.A. Emilio, M.I. Litter, J. Photochem. Photobiol. A Chem. 148 (2002) 223.
[33] J. Arana, O. Gonzalez Diaz, M. Miranda Saracho, J.M. Dona-Rodriguez, J.A. Herrera Melian, J. Perez Pena, Appl. Catal. B 32 (2001) 49.
[34] J. Arana, J.M. Dona-Rodriguez, O. Gonzalez Diaz, E. Tello Rendon, J.A. Herrera Melian, G. Colon, J.A. Navio, J. Perez Pena, J. Mol. Catal. A Chem. 215 (2004) 153.
[35] A. Henglein, J. Phys. Chem. 83 (1979) 2209.
[36] J.M. Herrmann, in: R.T.K. Baker, S.J. Tauster, J.A. Dumesic (Eds.), Strong Metal–Support Interactions, ACS Symposium Series, vol. 298, 1986, p. 200.
[37] J. Disdier, J.M. Herrmann, P. Pichat, J. Chem. Soc. Faraday Trans. I 77 (1981) 2815.
[38] Y. Liu, C. Liu, Q. Rong, Z. Zhang, Appl. Surf. Sci. 220 (2003) 7.
[39] C.A.K. Gouvea, F. Wypych, S.G. Moraes, N. Duran, P.P. Zamora, Chemosphere 40 (2000) 427.
[40] S. Chen, U. Nickel, Chem. Commun. 2 (1996) 133.
[41] V. Vamathevan, R. Amal, D. Beydoun, G. Low, S. McEvoy, J. Photochem. Photobiol. A Chem. 148 (2002) 233.
[42] H.M. Sung-Suh, J.R. Choi, H.J. Hah, S.M. Koo, Y. Chan Bae, J. Photochem. Photobiol. A Chem. 163 (2004) 37.
[43] S. Kato, Y. Hirano, M. Iwata, T. Sano, K. Takeuchi, S. Matsuzawa, Appl. Catal. B 57 (2004) 109.
[44] R. Wang, J.H. Xin, Y. Yang, H. Liu, L. Xu, J. Hu, Appl. Surf. Sci. 227 (2004) 312.
[45] T.T.Y. Tan, C.K. Yip, D. Beydoun, R. Amal, Chem. Eng. J. 95 (2003) 179.

[46] C. He, Y. Xiong, J. Chen, C. Zha, X. Zhu, J. Photochem. Photobiol. A Chem. 157 (2003) 71.
[47] J.M. Herrmann, H. Tahiri, Y. Ait-Ichou, G. Lassaletta, A.R.G. Elipe, A. Fernandez, Appl. Catal. B 13 (1997) 219.
[48] M. Moonsiri, P. Rangsunvigit, S. Chavadej, E. Gulari, Chem. Eng. J. 97 (2004) 241.
[49] H. Tada, T. Ishida, A. Takao, S. Ito, Langmuir 20 (19) (2000) 7898–9000.
[50] H. Gerischer, A. Heller, J. Phys. Chem. 95 (1991) 5261.
[51] E. Stathatos, P. Lianos, P. Falaras, A. Siokou, Langmuir 16 (2000) 2398.
[52] S. Sakthivel, M.V. Shankar, M. Palanichamy, B. Arabindoo, D.W. Bahnemann, V. Murugesan, Water Res. 38 (2004) 3001.
[53] Y. Nakaoka, Y. Nosaka, J. Photochem. Photobiol. A Chem. 110 (1997) 299.
[54] R.H. Howe, M. Gratzel, J. Phys. Chem. 91 (1987) 3906.
[55] P. Meriaudeau, J.C. Vedrine, J. Chem. Soc. Faraday Trans. 72 (1976) 472.
[56] T. Sano, N. Negishi, K. Uchino, J. Tanaka, S. Matsuzawa, K. Takeuchi, J. Photochem. Photobiol. A Chem. 160 (2003) 93.
[57] X.Z. Li, F.B. Li, Environ. Sci. Technol. 35 (2001) 2381.
[58] G. Zhao, H. Kozuka, T. Yoko, Thin Solid Films 277 (1996) 147.
[59] G. Lassaletta, A.R. Gonzales-Elipe, A. Justo, A. Fernandez, F.J. Ager, M.A. Respaldiza, J.G. Soares, M.F. Da Silva, J. Mater. Sci. 31 (1996) 2325.